Characterization of a Phanerochaete chrysosporium Glutathione Transferase Reveals a Novel Structural and Functional Class with Ligandin Properties

Yann Mathieu, Pascalita Prosper, Marc Buée, Stephane Dumarcay, Frederique Favier, Éric Gelhaye, Philippe Gerardin, Luc Harvengt, Jean-Pierre Jacquot, Tiphaine Lamant Dhalleine, et al.

THE JOURNAL OF BIOLOGICAL CHEMISTRY VOL. 287, NO. 46, pp. 39001–39011, November 9, 2012

Characterization of a *Phanerochaete chrysosporium* Glutathione Transferase Reveals a Novel Structural and Functional Class with Ligandin Properties*[S]

Received for publication, July 20, 2012, and in revised form, September 7, 2012 Published, JBC Papers in Press, September 24, 2012, DOI 10.1074/jbc.M112.402776

Yann Mathieu[‡§¶1], Pascalita Prosper[‖1], Marc Buée[§], Stéphane Dumarçay[‡‡], Frédérique Favier[‖**], Eric Gelhaye[‡§], Philippe Gérardin[‡‡], Luc Harvengt[¶], Jean-Pierre Jacquot[‡§], Tiphaine Lamant[‡§], Edgar Meux[‡§], Sandrine Mathiot[‖**], Claude Didierjean[‖**2], and Mélanie Morel[‡§3]**

*From the [‡]Université de Lorraine, Interactions Arbre-Microorganismes, UMR 1136, Institut Fédératif de Recherche 110 EFABA, Vandoeuvre-lès-Nancy F-54506, France, [§]Institut National de la Recherche Agronomique, Interactions Arbre-Microorganismes, UMR 1136, Vandoeuvre-lès-Nancy F-54506, France, [‖]Université de Lorraine, CRM2, UMR 7036, Vandoeuvre-lès-Nancy F-54506, France, **CNRS, CRM2, UMR 7036, Vandoeuvre-lès-Nancy F-54506, France, [‡‡]Université de Lorraine, Laboratoire d'Etudes et de Recherche sur le Matériau Bois, EA 1093, Vandoeuvre-lès-Nancy F-54506, France, and the [¶]Laboratoire de Biotechnologie, Pole Biotechnologie et Sylviculture Avancée, Institut Technologique Forêt Cellulose Bois-construction Ameublement, Campus Foret-Bois de Pierroton, 33610 Cestas, France*

Background: GSTs are detoxification enzymes poorly characterized in fungi.
Results: *GSTFuA1* possesses a unique three-dimensional structure and binds wood degradation compounds at or near the glutathione binding pocket.
Conclusion: This GST is a new fungal isoform that we name *GSTFuA1.*
Significance: GSTs with binding properties could be of great interest in various biotechnological applications.

Glutathione *S*-transferases (GSTs) form a superfamily of multifunctional proteins with essential roles in cellular detoxification processes. A new fungal specific class of GST has been highlighted by genomic approaches. The biochemical and structural characterization of one isoform of this class in *Phanerochaete chrysosporium* revealed original properties. The three-dimensional structure showed a new dimerization mode and specific features by comparison with the canonical GST structure. An additional β-hairpin motif in the N-terminal domain prevents the formation of the regular GST dimer and acts as a lid, which closes upon glutathione binding. Moreover, this isoform is the first described GST that contains all secondary structural elements, including helix α4′ in the C-terminal domain, of the presumed common ancestor of cytosolic GSTs (*i.e.* glutaredoxin 2). A sulfate binding site has been identified close to the glutathione binding site and allows the binding of 8-anilino-1-naphtalene sulfonic acid. Competition experiments between 8-anilino-1-naphtalene sulfonic acid, which has fluorescent properties, and various molecules showed that this GST binds glutathionylated and sulfated compounds but also wood extractive molecules, such as vanillin, chloronitrobenzoic acid, hydroxyacetophenone, catechins, and aldehydes, in the glutathione pocket. This enzyme could thus function as a classical GST through the addition of glutathione mainly to phenethyl isothiocyanate, but alternatively and in a competitive way, it could also act as a ligandin of wood extractive compounds. These new structural and functional properties lead us to propose that this GST belongs to a new class that we name GSTFuA, for fungal specific GST class A.

Glutathione *S*-transferases (GSTs) are a superfamily of proteins widespread in animals, plants, fungi, and bacteria. From a functional point of view, GSTs usually catalyze glutathione (GSH) transfer onto hydrophobic molecules (glutathionylation activity) or GSH removal from specific substrates (deglutathionylation) (1). These enzymes have broad substrate acceptance, although each GST possesses its own specific catalytic profile. Most GSTs are dimeric proteins. Each monomer is composed of a conserved thioredoxin domain containing the GSH binding pocket (G site) and a more variable α-helical domain (H site) containing the binding site for the GSH acceptor substrate (2). Most studies have focused on the GSH-dependent catalytic activities involved both in detoxification processes and endogenous metabolism. However, some GSTs have also been identified as proteins that selectively bind organic anions such as tetrapyrroles in mammals and plants (3–5). This "ligandin" property has been defined as the capacity of the protein to bind nonsubstrate ligands (3). In plants, it could be involved in the intracellular transport of hydrophobic compounds, such as pigments, and in temporary storage of phytohormones (6, 7). Fun-

* This work was supported by Convention industrielle de formation par la recherche (CIFRE) and Agence Nationale de la Recherche (ANR) Research Grant ANR-09-BLAN-0012; the Ministère de l'Enseignement Supérieur, de la Recherche, et de la Technologie; the Institut National de la Recherche Agronomique (INRA); and CNRS.
[S] This article contains supplemental Table 1 and Figs. S1–S11.
The atomic coordinates and structure factors (codes 4F03 and 4G19) have been deposited in the Protein Data Bank (http://wwpdb.org/).
The nucleotide sequence(s) reported in this paper has been submitted to the GenBank™/EBI Data Bank with accession number(s) JQ974949
[1] Both authors contributed equally to this work.
[2] To whom correspondence may be addressed: Université de Lorraine, UMR 7036 CRM2 Institut Jean Barriol, Faculté des Sciences et Technologies, BP 70239, 54506 Vandoeuvre-lès-Nancy Cedex, France. Tel.: 33-3-83-68-48-79; E-mail: Claude.Didierjean@crm2.uhp-nancy.fr.
[3] To whom correspondence may be addressed: Université de Lorraine, UMR 1136 "Interactions Arbres/Micro-organismes," Faculté des Sciences et Technologies BP 70239, 54506 Vandoeuvre-lès-Nancy Cedex, France. Tel.: 33-3-83-68-42-28; E-mail: mmorel@scbiol.uhp-nancy.fr.

gal GSTs have been less studied than their plant or animal counterparts. Nevertheless, the recent burst of fungal genome sequencing programs has highlighted evolutionary specificities of GSTs in these organisms (8–10). Currently, at least seven different classes of cytosolic GSTs have been defined in fungi: MAK16, EFBγ, Ure2p, Omega, *S*-glutathionyl-(chloro)hydroquinone reductase, GTT, and etherase-like. Although some isoforms from the Ure2p, Omega, *S*-glutathionyl-(chloro)hydroquinone reductase, and GTT have been characterized in yeast (11–13), *Aspergillus* sp. (14, 15), and *Phanerochaete chrysosporium* (9, 16), the etherase-like class has never been studied to date. Etherase-like GSTs are fungal specific, although they show weak homology with LigE, a bacterial protein responsible for the cleavage of β-aryl ether linkages of lignin in *Sphingobium* sp. SYK-6 (8, 17). The etherase-like class is expanded in wood decaying fungi, because, for instance, 11 etherase-like encoding genes are present in the genome of *Postia placenta*. Although less expanded, they are, however, present in pathogenic fungi as *Aspergillus* sp. or *Fusarium* sp. for example (8).

P. chrysosporium is a white rot fungus able to completely mineralize lignocellulose by degrading recalcitrant compounds. During the wood decaying process, phenolic acids and phenolic aldehydes are released. These compounds are problematic in biofuel production, but at the same time, they can have beneficial properties for human health. As an example, vanillin possesses antimicrobial activity, antioxidant properties, antimutagenic effects, and chemoprotective activity in inflammation and cancer (for a review, see Ref. 18). Syringaldehyde is also a naturally occurring aromatic compound, which exhibits both a detrimental action on cellulose hydrolysis and fermentation processes and a good antioxidant activity, being 2- and 10-fold more effective than quercetin and trolox, respectively (19).

In this study, we describe for the first time the biochemical and structural characterization of a GST belonging to the previously named "etherase-like" class in *P. chrysosporium* and demonstrate the ligandin property of this enzyme toward compounds derived from lignin degradation.

EXPERIMENTAL PROCEDURES

Materials—Hydroxyethyl disulfide was from Pierce. α-*O*-Methylumbelliferyl-β-hydroxylpropiovanillone was a gift from Dr. Masai (Nagaoka University of Technology, Japan). *S*-(phenylacetophenone)-glutathione and 2-methyl-*S*-glutathionyl-naphtoquinone were synthesized as described previously (16). *para*-Nitrophenyl sulfate potassium salt was from Acros Organics. 5-Chloromethylfluorescein diacetate (CMFDA)[4] was from Invitrogen. All other reagents were from Sigma-Aldrich.

Cloning of GST5118, GST5118-S22A, and GST5118-S22C—The enzyme studied here is referred to as GST5118 based on its protein identification number in the Joint Genome Institute database. The open reading frame sequence encoding *P. chrysosporium* GST5118 was amplified from a *P. chrysosporium* cDNA library using GST5118 forward and reverse primers (5′-CCCCCATGGCTCAGCCCATCGTGTT-3′ and 5′-CCCGGATCCCTATACATCAACCTGCT3′, respectively) and cloned into the NcoI and BamHI restriction sites (underlined in the primers) of pET-3d (Novagen). The amplified sequence encodes a protein in which an alanine has been inserted after the initiator methionine to improve protein production. Two mutants of the putative catalytic Ser-22 into Ala or Cys residues were also generated using two complementary mutagenic primers (supplemental Table 1).

Expression and Purification of the Recombinant Proteins—For protein production, the *Escherichia coli* BL21(DE3) strain, containing the pSBET plasmid, was co-transformed with the different recombinant plasmids (20). Cultures were progressively amplified up to 2 liters in LB medium supplemented with ampicillin and kanamycin at 37 °C. Protein expression was induced at exponential phase by adding 100 μM isopropyl β-D-thiogalactopyranoside for 4 h at 37 °C. The cultures were then centrifuged for 15 min at 4400 × *g*. The pellets were resuspended in 30 ml of TE NaCl (30 mM Tris-HCl, pH 8.0, 1 mM EDTA, 200 mM NaCl) buffer. Cell lysis was performed on ice by sonication (3 × 1 min with intervals of 1 min), and the soluble and insoluble fractions were separated by centrifugation for 30 min at 27,000 × *g* at 4 °C. All subsequent steps were performed in the cold. The soluble part was then fractionated with ammonium sulfate in two steps, and the protein fraction precipitating between 40 and 80% of saturation contained the recombinant protein, as estimated by 15% SDS-PAGE. The protein was purified by size exclusion chromatography after loading on an ACA44 (5 × 75-cm) column equilibrated in TE NaCl buffer. The fractions containing the protein were pooled, dialyzed by ultrafiltration to remove NaCl, and loaded onto a DEAE-cellulose column (Sigma) in TE (30 mM Tris-HCl, pH 8.0, 1 mM EDTA) buffer. The proteins were eluted using a 0–0.4 M NaCl gradient. Finally, the fractions of interest were pooled, dialyzed, concentrated by ultrafiltration under nitrogen pressure (YM10 membrane; Amicon), and stored in TE buffer at −20 °C. Purity was checked by SDS-PAGE. Protein concentrations were determined spectrophotometrically using a molar extinction coefficient at 280 nm of 68,870 M^{-1} cm^{-1}.

For the production of the selenomethionine-substituted GST5118, a methionine auxotroph strain, BL21(DE3)Met$^-$, was cotransformed with pET-GST5118 and pSBET. Cultures were done as described previously (21), and the labeled protein was purified following a procedure identical to that described for unlabeled GST5118.

Activity Measurements—The activity measurements of GST5118, GST5118-S22C, and GST5118-S22A proteins in thiol transferase activity with a hydroxyethyl disulfide assay or for reduction of dihydroascorbate were performed as described by Couturier *et al.* (22). The GSH transferase activity was assessed with phenethyl isothiocyanate (phenethyl-ITC) prepared in 2% (v/v) acetonitrile, 1-chloro-2,4-dinitrobenzene (CDNB), and 4-nitrophenyl butyrate (PNP-butyrate) prepared in DMSO. For these three substrates, the reactions were monitored at 274, 340, and 412 nm, respectively, following the increase in absorbance arising from the formation of the *S*-glutathionylated adduct. The reactions with CDNB and PNP-butyrate were performed in 100 mM phosphate buffer, pH 7.5, in

[4] The abbreviations used are: CMFDA, 5-chloromethylfluorescein diacetate; ANS, 8-anilino-1-naphtalene sulfonic acid; CDNB, 1-chloro-2,4-dinitrobenzene; ITC, isothiocyanate; PNP-butyrate, paranitrophenyl butyrate.

the presence of GSH (5 mM), whereas the reaction with phenethyl-ITC was performed at pH 6.5 with an identical GSH concentration. Esterase activity was measured in microplates using CMFDA as substrate, which releases fluorescence upon activation by esterases (23). Experiments were performed in 50 mM phosphate buffer, pH 8.0, in a total volume of 200 μl. The reactions were started by the addition of the purified enzyme, and fluorescence was measured every minute for 1 h with excitation at 485 nm and emission at 535 nm on a VICTOR™ *X*5 plate reader (PerkinElmer Life Sciences). Catalytic parameters were calculated using the GraphPad® software from steady state experiments performed using 0–25 μM CMFDA and 5 mM GSH.

Peroxidase activities were monitored as follows. 1 mM peroxide (hydrogen peroxide, *tert*-butyl hydroperoxide, and cumene hydroperoxide) in 30 mM Tris-HCl, pH 8.0, was incubated in the presence of 2 mM GSH, 200 μM NADPH, 0.5 IU of glutathione reductase. The activity was followed by monitoring the decrease in absorbance arising from NADPH oxidation in this coupled enzyme assay system, showing the formation of oxidized glutathione (GSSG). The reactions were started by the addition of the purified enzyme and monitored with a Cary 50 UV-visible spectrophotometer (VARIAN). To determine the catalytic properties of the enzyme, steady state assays were performed using variable substrate concentrations (from 10 μM to 10 mM), and the catalytic parameters were calculated using the GraphPad® software. Etherase activity was assessed according to Masai *et al.* (17). Sulfatase activity was performed with *para*-nitrophenyl sulfate potassium salt as described by Kim *et al.* (24).

Mass Spectrometry Analysis—GST5118 wild type and mutants were analyzed by Q-TOF MS as described by Koh *et al.* (25). When oxidation or reduction was required, proteins were treated at 25 °C for 60 min, whatever the reductant (dithiothreitol (DTT)) or the oxidant (GSSG) used. Excess of oxidant/reductant was removed using a Sephadex® G25 (GE Healthcare) gel filtration column.

8-Anilino-1-naphtalene Sulfonic Acid (ANS) Binding and Ligand Screening—All binding and competition experiments were performed in TE buffer, pH 8.0. ANS binding onto GST5118 and GST5118-S22C (DTT-treated or not) was investigated by monitoring fluorescence upon the addition of 50 μM ANS to 3 μM protein using a Cary Eclipse (VARIAN) fluorescence spectrophotometer. The excitation wavelength was set at 385 nm, and the emission spectra were recorded from 400 to 700 nm. Additional tryptophan-based fluorescence experiments were performed with GST5118 and GST5118-S22C in the presence or absence of 50 μM ANS. After excitation at 290 nm, emission spectra were recorded from 305 to 560 nm. The ANS binding site was investigated in the same conditions with 1 mM GSH, 5 mM phenethyl-ITC, or 50 μM CMFDA.

The correlation between ANS concentration and fluorescence yield was obtained by incubating 100 μM GST5118 with 1 μM ANS, giving the maximal value for 1 μM ANS bound onto the protein. Fluorescence from samples containing ANS alone was subtracted as a background. GST5118 was then incubated at a concentration of 3 μM with increasing concentrations of ANS ranging from 0 to 1 mM. To determine the dissociation constant of ANS, the following equation (Equation 1) was applied.

$$y = B_{max} \times [\text{Free ANS}]/(K_d + [\text{Free ANS}]) \quad \text{(Eq. 1)}$$

where y represents the specific binding (*i.e.* the concentration of ANS bound/protein) and B_{max} is the number of maximum specific binding sites.

Competition experiments were performed in a total volume of 250 μl containing 3 μM enzyme, 50 μM ANS, and various putative ligands (from 1 μM to 10 mM). Fluorescence emission from protein-free samples containing ANS and potential ligand were subtracted as background. A decrease in fluorescence, indicating competition between ligand and ANS, was measured after 10 min of incubation with excitation at 355 nm and emission at 460 nm on a VICTOR™ *X*5 plate reader (PerkinElmer Life Sciences). IC_{50} values were obtained by fitting data to Equation 2,

$$Y = Bottom + (Top - Bottom)/(1 + 10^{(\text{Log[Ligand]} - \text{Log IC}_{50})}) \quad \text{(Eq. 2)}$$

where Y represents the fluorescence signal observed after background subtraction, *Top* is the fluorescence signal of ANS bound onto GST5118 without any ligand, and *Bottom* is the fluorescence signal of ANS at the highest ligand concentration.

Inhibition Kinetics—Competition tests between ANS and phenethyl-ITC or CMFDA were performed by measuring GSH transferase and esterase activities. Activity with phenethyl-ITC was monitored in a total volume of 500 μl containing 50 μM GSH, 50 μM ANS, and 10 μM to 10 mM phenethyl-ITC. Inhibition tests of esterase activity with CMFDA by ANS or vanillin were performed in a total volume of 200 μl with or without 50 μM GSH, 50 μM ANS, or 300 μM vanillin and CMFDA (0 μM to 25 μM). Similar tests were performed with 25 μM CMFDA, 300 μM vanillin, and 0–5 mM GSH. The reactions were started by the addition of the purified enzyme, and the catalytic parameters were calculated using the GraphPad® software.

Crystallization—Two different samples were crystallized, the selenomethionine derivative protein (apoGST5118) and the native protein with bound GSH (holoGST5118). The crystallization experiments were set up using the microbatch under oil (paraffin) method at 277 K. Selenomethionine-apoGST5118 crystals appeared after 4–5 days from droplets containing 2 μl of protein solution (15–20 mg/ml protein in TE buffer) and 2 μl of precipitating solution (30% PEG 8000, 200 mM sodium acetate, and 100 mM sodium cacodylate, pH 6.5). Crystals of GST5118 in complex with GSH (holoGST5118) were obtained in co-crystallization experiments. The best crystals grew after 2 months in droplets containing a mixture of 485 μM protein solution (14 mg/ml) and 6 mM GSH in TE buffer and precipitating solution (30% PEG 8000, 200 mM sodium acetate, and 100 mM HEPES, pH 7.0). Prior to data collection, the crystals were transferred to a cryosolution containing 20% glycerol with mother liquor and flash-cooled to 100 K.

Data Collection and Processing, Structure Solutions, and Refinements—ApoGST5118 diffraction data were collected on the synchrotron beamline PX1 at SOLEIL (France) at 0.97918 Å, and holoGST5118 x-ray data were measured on the beam-

TABLE 1
Statistics of x-ray diffraction data collection and model refinement

	ApoGST5118	HoloGST5118
Data collection		
Beam line	PX1, SOLEIL	BM30A/FIP, ESRF
Space group	$P2_12_12_1$	$P2_12_12_1$
No. of dimers in the asymmetric unit	2	2
Cell dimensions *a*, *b*, *c* (Å)	86.05 88.46 157.16	86.57 88.15 156.49
Resolution (Å)	44.23–1.80 (1.89–1.80)[a]	48.48–2.00 (2.11–2.00)
R_{merge}	0.08 (0.619)	0.069 (0.375)
Mean $I/\sigma(I)$	22.2 (3.6)	20.0 (4.7)
Completeness (%)	99.7 (98.1)	100.0 (99.9)
n observations	1,443,573 (112,670)	555,508 (71,179)
Redundancy	12.8 (7.2)	6.8 (6.0)
Wilson *B* factor (Å^2)	20.1	21.8
Phasing method	**SAD**[b]	
Refinement		
Resolution (Å)	42.54–1.80 (1.84–1.80)	44.90–2.00 (2.02–2.00)
n reflections	111,495 (7,219)	81,509 (2,780)
Cut-off	$F > 0\sigma(F)$	$F > 0\sigma(F)$
R_{all} (%)[c]	19.3	17.8
R_{free} (%)[d]	22.7 (30.1)	22.1 (32.5)
Average *B*-factor (Å^2)		
Protein atoms	25.1	24.6
Ligand atoms	28.1	30.6
Solvent atoms	29.7	31.2
Ramachandran statistics (%)		
Residues in preferred regions	98.5	98.6
Residues in allowed regions	1.1	1.0
Outlier residues	0.4	0.4
Root mean square deviations		
Bond length (Å)	0.007	0.007
Bond angle (degrees)	1.025	1.034

[a] Values in parentheses are for highest resolution shell.
[b] Single-wavelength anomalous dispersion.
[c] R_{all} was determined from all of the reflections (working set + test set), whereas R_{free} corresponds to a subset of reflections (test set).

line BM30A/FIP at the European Synchrotron Radiation Facility (Grenoble, France) at 0.97854 Å. The data sets were processed with XDS (26) and scaled with SCALA (27) from the CCP4 package (28). The molecular replacement method failed to solve the protein structure, probably because the best templates share less than 30% sequence identity with GST5118. The apoGST5118 structure was solved by the single-wavelength anomalous dispersion method using Phenix AutoSol (29). The eight expected selenium atoms were found using SOLVE (30), and resulting single-wavelength anomalous dispersion phases had a figure of merit of 0.38. A nearly complete backbone trace was obtained automatically with RESOLVE (30). ApoGST5118 and holoGST5118 models were refined using PHENIX (29) and manually corrected using COOT (31). The validations of GST5118 crystal structures were automatically performed with MOLPROBITY (32) from PHENIX (29). Final model statistics are shown in Table 1.

ApoGST5118 and holoGST5118 crystals belonged to the space group $P2_12_12_1$, and the asymmetric unit consisted of four polypeptide chains. Non-denaturant liquid chromatography and crystal packing analysis using PISA (33) showed that both proteins are homodimeric. The asymmetric unit content corresponds to two dimers where the two protomers are related to each other by a noncrystallographic 2-fold symmetry axis. The electron density maps of holoGST5118 revealed unambiguously the presence of one GSH molecule per monomer. In the apo structure, an electron density peak was found in the active site, identified as a sulfate ion arising most probably from the ammonium fractionation step used during purification. In the holo structure, the corresponding electron density peak was clearly weaker and was interpreted as an acetate ion from the crystallization solution (supplemental Fig. S1). The quality of the final electron density maps is shown in supplemental Fig. S2.

Structural comparisons were done using the DALI structural alignment server (34) and the program Strap (35). Figures of molecular models were prepared with PyMOL. The root mean square deviations between protein structures were calculated with PyMOL or DALI. Secondary structure predictions were carried out with the server Jpred3 (36). The multiple-sequence alignment figure (supplemental Fig. S6) was prepared using Espript (37).

RESULTS

GST5118 X-ray Structures—Two structures of GST5118 (apo and holo with bound GSH) were solved by using the single-wavelength anomalous diffraction data collected from crystals of the selenomethionylated protein. Each corresponded to the same local packing with two homodimers arranged similarly in the asymmetric units. In each structure, the four monomers adopted quite similar structures. Average root mean square deviations of the six possible superpositions are 0.34 and 0.27 Å for apo and holo structures, respectively. Root mean square deviations increased by at least 0.2 Å when apo and holo monomers were compared. This increase is mainly contributed by the displacement of β-hairpin $\beta2'\beta2''$ during the apo-holo transition (see below).

The GST5118 monomer adopts the GST canonical fold, which consists of an N-terminal thioredoxin-like motif ($\beta1\alpha1\beta2\alpha2\beta3\beta4\alpha3$) and a C-terminal domain of at least four helices ($\alpha4\alpha5\alpha6\alpha7$). The two most conserved residues in GST

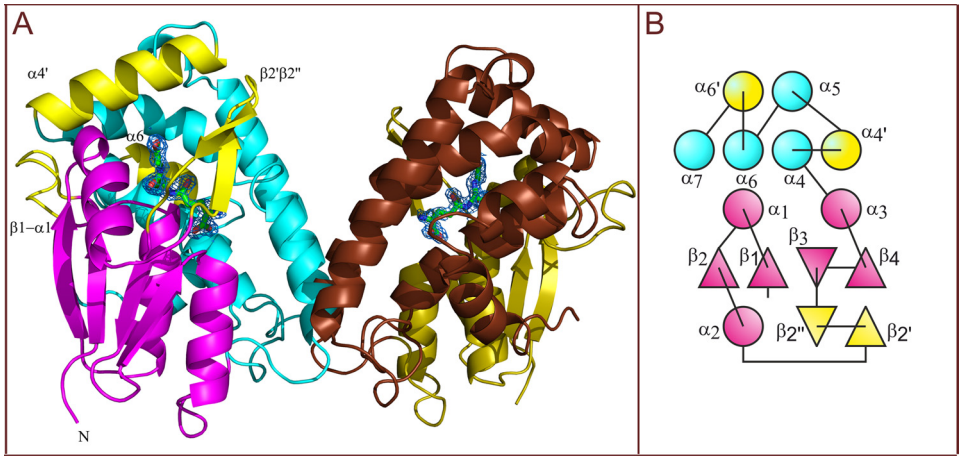

FIGURE 1. **Unique dimeric organization of GST5118.** *A*, view of the original dimer of GST5118. The additional secondary structures, highlighted in *yellow* in the *left* monomer, include an elongation of the β1-α1 loop, a β-hairpin motif in the α2-β3 loop, and the α-helices α4′ and α6′. In the *left* monomer, the N- and C-terminal domains are *colored* in *magenta* and *cyan*, respectively; in the *right* monomer they are *colored* in *olive* and *chocolate*, respectively. Both monomers have the ability to bind one glutathione molecule, depicted as *green sticks*, with corresponding $2F_o - F_c$ electron density (contour level 1.2 σ). *B*, topology diagrams of GST5118 (*circles*, helices; *triangles*, strands). The regular secondary structures of GSTs are *colored cyan* and *magenta*, whereas original elements are *colored yellow*.

are present in GST5118: *cis*-Pro-74 in the N-terminal domain, which is assumed to maintain the enzyme in a catalytically competent structure (38), and Asp-205, which is important for the C-terminal domain cohesion through its participation in the N-capping box (39). Nevertheless, the GST5118 structure contains unique features in both N- and C-terminal domains (Fig. 1). The first one is an elongation of about 8 residues of the loop β1-α1 (11–22) when compared with almost all GSTs. Only GST-like chloride intracellular channel proteins and the recently characterized GST from *Agrobacterium tumefaciens* (40) exhibit this property. In both GST5118 and *A. tumefaciens* GST structures, this long β1-α1 loop closes one part of the electrophilic substrate pocket (H site). In addition, a β-hairpin motif (β2′β2″) between α2 and β3 is observed for the first time in a GST fold. This motif hinders the formation of the regular GST dimer and partially covers the GSH binding site (G site). The C-terminal domain includes two extra helices: α4′, which follows α4 in an antiparallel way, and α6′ located between α6 and α7. This second supplementary helix is a characteristic of plant Phi GSTs (41). As for helix α4′, to the best of our knowledge, it has been observed only in GRX2 (glutaredoxin 2) (Protein Data Bank entries 3ir4 and 1g7o (42)). This protein is assumed to be the common ancestor of GSTs (43). Furthermore, α4′ lies in a position similar to the C-terminal helix of the human Alpha and Theta GSTs (supplemental Fig. S3). It has been proposed that a secondary structure in this position covers the H site and reduces its accessibility (44, 45).

GST5118 exhibits a new dimerization mode with an accentuated open V-shape where both subunits are related by a *C2* symmetry. In the canonical GST assembly, the α4 and α5 helices of one monomer pack against the N-terminal domain of its partner. In GST5118, the additional β-hairpin prevents this proximity. Helix α4 of one subunit packs in the groove between helices α4 and α5 of the other protomer (Fig. 1 and supplemental Fig. S4). Interestingly, this new oligomeric structure conserves a large cleft in the center of the dimer facing both of the active sites. The size of the buried interface (1850 Å^2) is significant and comparable with that observed in the "open" classical GST dimers like in human Omega GST (46) or in *Drosophila* Sigma GST (47). There are five hydrogen bonds and a hydrophobic lock-and-key motif that hold the two protomers together. The key residue of the lock-and-key motif is Phe-113 from helix α4. It fits in the pocket of the other subunit formed by Pro-107 from loop α3-α4; Gln-114 and Phe-117 from helix α4; Leu-195, Met-196, and Thr-203 from the α5-α6 loop; and Ser-205 from helix α6 (supplemental Fig. S5). Interestingly, this motif is present in Alpha, Mu, and Pi GSTs (48), where the lock is also located between helices α4 and α5. However, in the latter cases, the key is located in loop α2-β3, which is replaced by the protruding β-hairpin in GST5118.

In the catalytic center of the holo structure, the GSH molecule fits in the canonical G site, where the anchoring motifs for the γ-glutamyl and cysteinyl moieties are conserved in GSTs from this class. The imidazole group of His-70, from the β-hairpin motif, interacts via a water molecule with the carbonyl group of the γ-glutamyl moiety and with the amide group of the glycyl moiety (Fig. 2). Its carboxylate group is stabilized by the side chains of Tyr-148 and Arg-153 from α4′. The thiol sulfur of GSH forms a hydrogen bond with the hydroxyl group of the putative catalytic Ser-22, which is located at the N-terminal end of α1 in the thioredoxin domain. This Ser-22 occupies the same position as the catalytic residue of the Cys/Ser-GSTs (supplemental Fig. S3). The two residues Trp-21 and Pro-23, which surround the above-mentioned catalytic serine and take part in the H site, are invariant in GSTs from this class (supplemental Fig. S6). Trp-21 is a very well conserved residue in thioredoxins that is involved in enzyme substrate recognition (49), and Pro-23 is a well conserved residue in the active site motif in the class I glutaredoxins (50).

Upon GSH binding, significant conformational changes occur in the GST5118 structure. In the G site, the β-hairpin motif comes closer to the glycyl moiety, allowing its interaction with the side chain of His-70, which adopts a new rotamer (from m-70 to t60). The side chain conformation of Asp-87 also changes to stabilize the N-terminal end of GSH (from t70 to t0). In the H site, Trp-122 and Phe-127 from α4 undergo confor-

mational changes that could improve the electrophilic substrate accessibility (Fig. 2).

In the apoGST5118 form, a heavy residual peak of electron density was found in the vicinity of the putative catalytic Ser-22. It was assigned to a sulfate ion, which is stabilized by the side chains of Tyr-46 (α2) and Arg-153 (α4′). In a similar position, a sulfate binding site was reported in the crystal structures of human Theta GST (45), human Zeta GST (51), and yeast elongation factor 1Bγ (52). In order to stabilize the sulfate anion, the role of Arg-153 (α4′) of GST5118 is played by Arg-239 of human Theta GST located in the C-terminal helix (supplemental Fig. S3). It is important to stress that both residues are located roughly in the same spatial position although not in the same secondary structure. A catalytic role was attributed to the anion binding site in human GST T2-2, which displayed a sulfatase activity toward aralkylsulfates (45).

GST5118 Activities—Glutathionylation activity of GST5118 has been tested using CDNB, phenethyl-ITC, 4-nitrophenyl butyrate (PNP-butyrate), and CMFDA as substrates (Table 2). CMFDA is a molecule releasing fluorescence upon activation by esterases (23). GST5118 is active at transferring GSH onto phenethyl-ITC and PNP-butyrate but not CDNB. Surprisingly, GST5118 also exhibits two types of esterase activity on CMFDA, one with and another one without GSH (Table 2). Still, in the absence of GSH, the activity remains weak, with a catalytic efficiency 12-fold lower than in the presence of GSH. By contrast, no thiol transferase activity could be detected with hydroxyethyl disulfide, and the enzyme was also inactive in the reduction of dehydroascorbate. In addition, no peroxidase activity could be detected with either hydrogen peroxide, *tert*-butyl hydroperoxide, or cumene hydroperoxide. Etherase activity was also tested using the synthetic substrate α-*O*-methylumbelliferyl-β-hydroxylpropiovanillone. This compound is an analog of lignin fragments containing an ether linkage that can be cleaved by Lig proteins (17). Using LigF from *Sphingobium* sp. SYK-6 as control (53), we showed that GST5118 does not possess etherase activity with α-*O*-methylumbelliferyl-β-hydroxylpropiovanillone. GST5118 does not display sulfatase activity using *para*-nitrophenyl sulfate potassium, although a sulfate binding site has been identified in the structure.

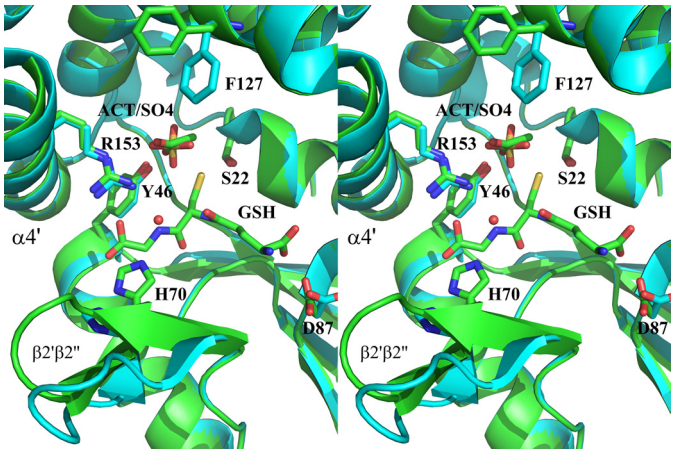

FIGURE 2. **Stereo view of the active site of GST5118.** The apo and holo forms are shown *superimposed* in order to highlight the conformational changes upon GSH binding. The anion binding site of GST5118 contains a sulfate ion in the apo form and an acetate ion in the holo form. The carbon atoms of the GSH-liganded and unliganded forms are *colored cyan* and *green*, respectively. Other atoms are *colored* according to their types. For clarity, only selected residues of the active site are shown and labeled.

Based on sequence alignments and structural data, we postulated that Ser-22 (GST5118 numbering) could be the catalytic residue responsible for GST5118 activity. Two directed mutations have been performed replacing Ser-22 by an alanine (GST5118-S22A) or a cysteine (GST5118-S22C). Both proteins lost GSH transferase activity using phenethyl-ITC. Surprisingly, GST5118-S22A gained activity with CDNB, hydroxyethyl disulfide, and cumene hydroperoxide (Table 2). On the other hand, GST5118-S22C was inactive with all substrates used in this study (data not shown).

ANS Binding Site—ANS is an environment-sensitive fluorescent dye, the fluorescence quantum yield of which increases upon binding to hydrophobic sites of proteins (54). ANS binding onto GST5118 was accompanied by the appearance of a characteristic fluorescence emission spectrum with a maximum at 475 nm, the excitation wavelength being fixed at 385 nm (Fig. 3*A*). The fluorescence signal, resulting from the interaction between the protein and ANS, was established rapidly in less than 30 s and increased with the molar ratio of ANS to GST5118, revealing a saturation curve. For concentrations

TABLE 2

Kinetic parameters of GST5118 and GST5118-S22A in enzymatic assays

The apparent K_m values for all compounds were determined using a concentration range of 0.1–10 mM in the presence of 2 mM GSH for GST5118 and 5 mM for GST5118-S22A. The K_m value for GSH was determined with 600 μM Phenethyl-ITC for GST5118 and 1 mM PNP-butyrate for GST5118-S22A and a concentration range of 0.01–10 mM GSH. The apparent K_m and k_{cat} values were calculated by nonlinear regression using the Michaelis-Menten equation ($r^2 > 0.99$). Data are represented as mean ± S.D. ($n = 3$). ND, not detected. The detection limit was estimated at 0.5 mIU. GOUαO, α-*O*-methylumbelliferyl-β-hydroxyl-propiovanillone.

Substrate	K_m		k_{cat}		k_{cat}/K_m	
	GST5118	GST5118-S22A	GST5118	GST5118-S22A	GST5118	GST5118-S22A
	μM		min^{-1}		min^{-1} μM^{-1}	
CDNB	ND	653.8 ± 49.4	ND	1765.0 ± 115.6	ND	2.69 ± 0.02
HED	ND	178.6 ± 7.8	ND	57.3 ± 6.8	ND	0.32 ± 0.02
DHA	ND	ND	ND	ND	ND	ND
Phenethyl-ITC	119.0 ± 14.4	ND	510.9 ± 16.0	ND	4.3 ± 0.3	ND
H_2O_2	ND	ND	ND	ND	ND	ND
Tertbutyl-OOH	ND	ND	ND	ND	ND	ND
Cu-OOH	ND	3767.0 ± 437.0	ND	62.6 ± 1.5	ND	0.011 ± 0.002
GOUαO	ND	ND	ND	ND	ND	ND
PNP-butyrate	774.3 ± 88.3	190.7 ± 24.1	165.0 ± 5.6	17.6 ± 0.5	0.21 ± 0.01	0.092 ± 0.005
CMFDA without GSH	3.6 ± 0.6	1.1 ± 0.1	0.0060 ± 0.0002	0.27 ± 0.01	0.0017 ± 0.0002	0.24 ± 0.01
CMFDA with GSH	8.0 ± 0.8	1.5 ± 0.1	0.17 ± 0.04	1.20 ± 0.06	0.021 ± 0.002	0.80 ± 0.02
GSH	216.4 ± 34.9	615.4 ± 44.2	662.0 ± 14.2	13.8 ± 0.6	3.1 ± 0.4	0.022 ± 0.002

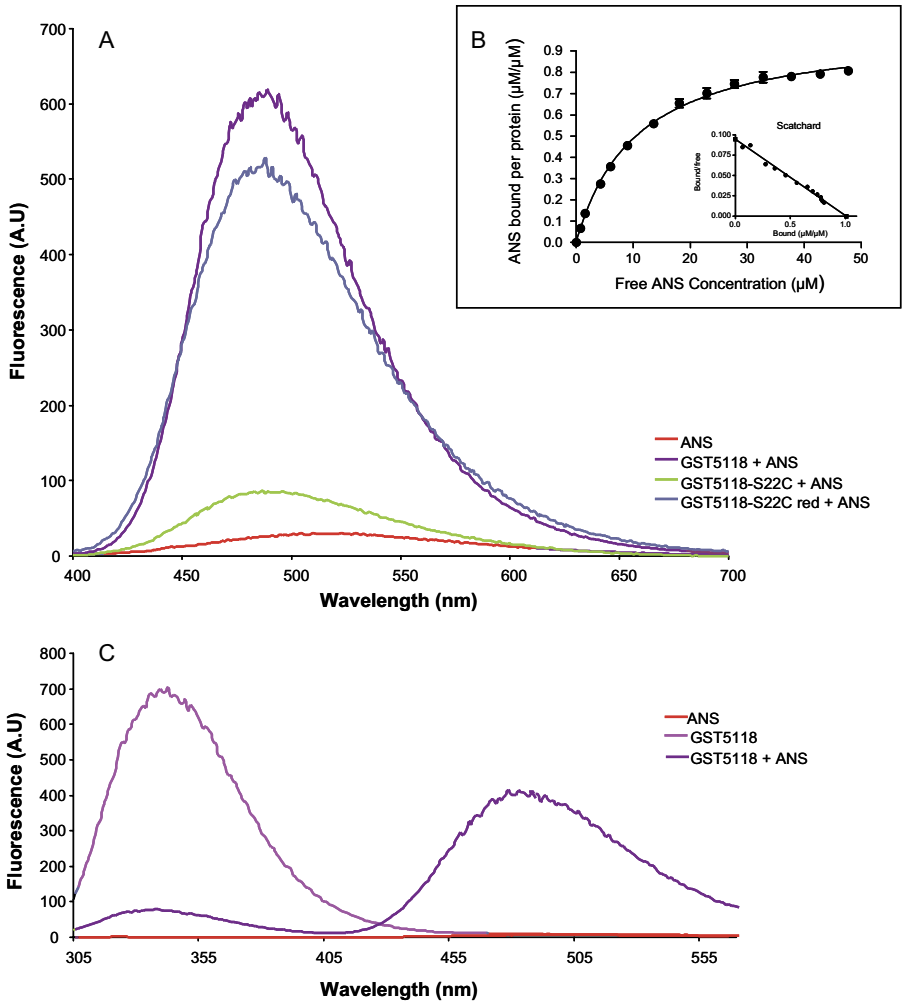

FIGURE 3. **ANS binding onto GST5118.** *A*, comparison of the fluorescence spectra (excitation at 385 nm) of 50 μM ANS bound onto GST5118 and GST5118-S22C DTT-treated (reduced) or not. Emission spectrum of 50 μM ANS alone is reported. *B*, binding saturation of GST5118 with ANS and Scatchard plot. *C*, tryptophan-based fluorescence (excitation at 290 nm, emission at 340 nm) of GST5118 alone and upon the addition of ANS. The emission spectrum of 50 μM ANS alone is reported. Data are represented as mean ± S.D. (n ± 3). *A.U.*, absorbance units.

higher than 50 μM ANS, a loss of signal was observed as previously shown for BSA or MurA interaction with ANS (54). A dissociation constant of 10.65 ± 0.5 μM was obtained by plotting the concentration of ANS bound onto GST5118 against the concentration of free ANS. Data were fitted to Equation 1. The number of ANS binding sites, determined as described under "Experimental Procedures," was 1.008 ± 0.015, suggesting the binding of only one ANS molecule per monomer (Fig. 3*B*).

In additional experiments, tryptophan-based fluorescence of GST5118 was measured using 290 and 340 nm as excitation and emission wavelengths, respectively, in the presence or absence of ANS (Fig. 3*C*). Fluorescence resonance energy transfer (FRET), revealed by the appearance of a signal at 475 nm, was observed between Trp and ANS, confirming the binding of ANS onto the protein, the energy transfer being highly dependent on the distance between the donor and acceptor molecules (Fig. 3*C*). This result is in accordance with the presence of four Trp residues in the vicinity of the Ser-22 (Trp-21, Trp-26, Trp-122, and Trp-215).

Similar experiments have been performed using the mutated protein GST5118-S22C. Interestingly, the GST5118-S22C mutant is able to bind ANS only after reduction with DTT (Fig. 3*A*). Besides giving information about the ANS binding site in GST5118, these data demonstrate the robustness of the method. Mass spectrometry experiments performed on GST5118-S22C showed that it covalently binds a GSH adduct. Indeed, purified GST5118-S22C exhibited a molecular mass of 29,033 Da, whereas the previously DTT-treated protein exhibited the expected molecular mass calculated from the primary sequence of 28,728 Da. Additionally, after treatment with GSSG, *S*-(phenylacetophenone)-glutathione, and 2-methyl-*S*-glutathionyl-naphtoquinone, the mass of the reduced protein increased by 305 Da (29,033 Da), which corresponds to a GSH adduct. By contrast, no GSH adduct was detected on the wild type protein, suggesting that the mutated protein is able to bind GSH covalently at the newly added cysteinyl residue, this addition preventing ANS binding onto the protein. ANS binding onto GST5118 was investigated in the presence of various GSH concentrations (up to 10 mM), demonstrating that GSH inhibits ANS binding. The obtained data were fitted to Equation 2, leading to an IC_{50} value of 261.5 ± 39.8 μM (supplemental Fig. S7). This measured value is in accordance with the K_m for GSH (216.4 ± 34.89 μM) found in the enzymatic assays. Additionally,

TABLE 3

Competition experiments between ANS and various compounds

Values given are IC_{50} fluorescence inhibition obtained by fitting data to Equation 2. Menadione-SG, 2-methyl-*S*-glutathionyl-naphtoquinone.

	GST5118
K_d ANS	10.6 ± 0.5 μM
No. of fixation sites at 50 μM ANS	1.008 ± 0.015
Glutathione	261.5 ± 39.8 μM
Beech compounds	
Coniferaldehyde	61.3 ± 1.2 μM
Vanillin	216.6 ± 8.5 μM
2-Hydroxy-4-methoxybenzophenone	–
4-Chloro-3-nitrobenzoic acid	1.5 ± 0.1 mM
4′-Hydroxyacetophenone	2.3 ± 0.4 mM
Gallic acid	–
Vanillic acid	–
Epicatechin	1.7 ± 0.1 mM
Syringaldehyde	79.4 ± 1.6 μM
Catechin hydrate	584.3 ± 98.7 μM
3-Hydroxy-4-methoxycinnamic acid, predominantly *trans*	–
Glutathionylated compounds	
2-Bromo-4′-phenylacetophenone	
Phenylacetophenone-SG	99.7 ± 46.5 μM
Menadione	–
Menadione-SG	83.7 ± 38.4 μM
Sulfated compounds	
1,2-Naphtoquinone-4-sulfonic acid	334.5 ± 56.8 μM
p-Xylene-2-sulfonic acid hydrate	928.7 ± 258.8 μM
p-Xylene	–
4-Aminotoluene-3-sulfonic acid	1.6 ± 0.5 mM
4-Methylumbelliferyl-sulfate	223.6 ± 25.3 μM
4-Methylumbelliferone	–

excitation transfer between Trp and bound ANS was fully abolished in the presence of 1 mM GSH (supplemental Fig. S8). *S*-(phenylacetophenone)-Glutathione and 2-methyl-*S*-glutathionyl-naphtoquinone were also able to inhibit ANS binding, whereas the same compounds deprived of the GSH adduct could not (Table 3). Taking together, these data suggest strongly that in GST5118, the ANS binding site overlaps at least in part the glutathione binding site (G site).

In the vicinity of catalytic Ser-22, a sulfate/acetate binding site has been detected in the GST5118 structure. Because ANS possesses a sulfonic acid motif, various sulfated compounds were tested for their ability to interact with the ANS binding site in GST5118. ANS binding is inhibited in the presence of 4-aminotoluene-3-sulfonic acid, *p*-xylene-2-sulfonic acid hydrate, 1,2-naphtoquinone-4-sulfonic acid sodium, and also 4-methylumbelliferyl sulfate potassium (Table 3). Moreover, this inhibition seems to be sulfate/sulfonate-dependent because 4-methylumbelliferone and *p*-xylene do not compete with ANS, suggesting that the ANS binding site also overlaps with the sulfate-binding site in GST5118.

Competition experiments between ANS and various substrates have been performed in order to investigate possible overlapping between the substrate binding site and the ANS binding site. As shown above, GST5118 exhibits a relatively high affinity for CMFDA, phenethyl-ITC, and PNP-butyrate with and without GSH (Table 3). ANS binding onto GST5118 remained mainly unaltered in the presence of either phenethyl-ITC or CMFDA (supplemental Fig. S9). Moreover, GST5118 activity against phenethyl-ITC is inhibited in the presence of ANS (supplemental Fig. S10). Concerning CMFDA, only esterase activity with GSH is inhibited by ANS (Fig. 4*A*). Due to quenching phenomena, PNP-butyrate was not used in this test.

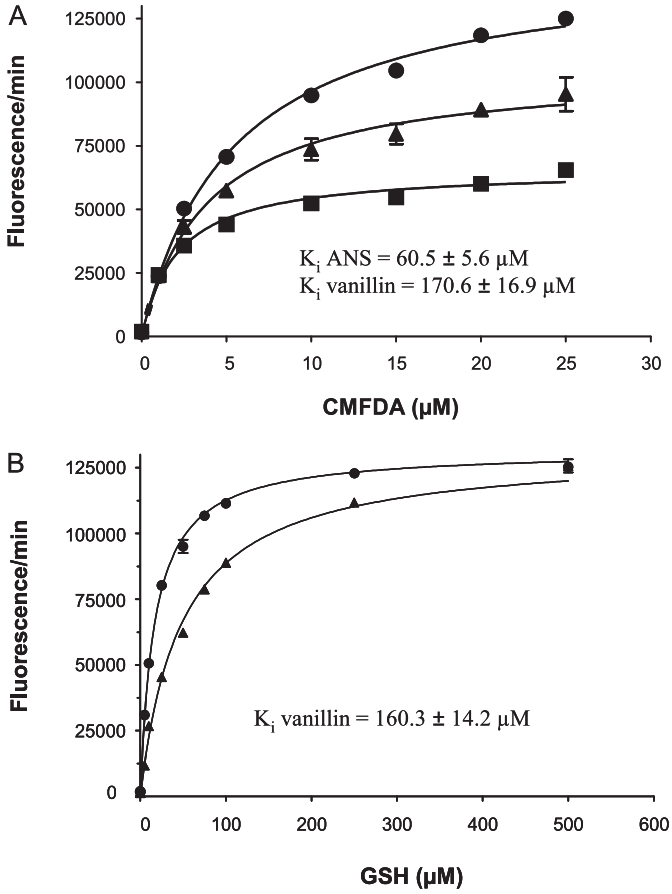

FIGURE 4. **Inhibition of GSH-dependent esterase activity by ANS or vanillin.** Data are represented as mean ± S.D. ($n \pm 3$). *A*, noncompetitive inhibition of esterase activity against CMFDA without inhibitor (●) or in the presence of 50 μM ANS (■) or 300 μM vanillin (▲). K_i values were calculated resolving to the non-linear noncompetitive inhibition equation ($r^2 > 0.99$): $V_{maxinh} = V_{max}/(1 + I/K_i)$; $Y = V_{maxinh} \times X/(K_m + X)$. V_{max} and K_m represent the maximum enzyme velocity and the Michaelis-Menten constant without inhibitor, whereas V_{maxinh} represents the maximum enzyme velocity for one concentration of inhibitor, and K_i is the inhibition constant. *B*, competitive inhibition of esterase activity GSH-dependent against GSH without inhibitor (●) or in the presence of 300 μM vanillin (▲). The K_i value was calculated resolving to the non-linear competitive inhibition equation ($r^2 > 0.99$): $K_{m(obs)} = K_m \times (1 + [I]/K_i)$; $Y = V_{max} \times X/(K_{m(obs)} + X)$. V_{max} and K_m represent the maximum enzyme velocity and the Michaelis-Menten constant without inhibitor, whereas $K_{m(obs)}$ represents the Michaelis-Menten constant in the presence of inhibitor, and K_i is the inhibition constant.

Taken together, these data suggest that the ANS binding site does not overlap with the substrate binding site because the probe does not compete with hydrophobic substrates as phenethyl-ITC or CMFDA for binding. By contrast, the competition between ANS and GSH (Fig. 4*B*) and the inhibition of GSH-requiring activities show an overlap between ANS and the G site of GST5118.

Ligand Screening—Using ANS as a screening tool, competition experiments have been performed with 11 structurally variable beech compounds (supplemental Fig. S11). Seven of them were recognized by GST5118 (Table 3). Among these products, those exhibiting the better affinity for GST5118 are either aldehydes or compounds harboring electrophilic motifs or atoms such as chlorine or nitrogen. Steric hindrance is not a factor influencing ligand binding because epicatechin and catechin hydrate, two of the largest compounds used, are both bound by GST5118.

To confirm the interaction between these compounds and GST5118, additional experiments were conducted using vanillin and testing the ability of GST5118 to react with CFMDA in the presence and absence of glutathione. Vanillin strongly inhibited the activity in the presence of GSH (Fig. 4) but had no effect in the absence of GSH (data not shown). Kinetic experiments revealed, as expected, a non-competitive inhibition against CFMDA (*i.e.* different binding sites for vanillin and CFMDA) and a competitive inhibition against GSH (*i.e.* overlapping binding sites for vanillin and GSH). In both cases, the K_i value (K_i around 200 μM) is in accordance with the IC_{50} value calculated from the experiments performed with ANS (216.6 ± 8.5 μM).

As summarized in Fig. 5, all of these data suggest that GSH, ANS, sulfate/acetate, and ligands such as vanillin bind to GST5118 through overlapping binding sites, which are different from the substrate-binding site.

DISCUSSION

GST5118 is a newly identified fungal GST with unique properties both in terms of structural organization and biochemistry. GST5118 monomer exhibits two extra secondary structures in addition to the canonical GST framework: 1) the β-hairpin $\beta2'\beta2''$ in the N-terminal domain, which hinders the formation of the regular GST dimer and which may be described as a shield covering the G site once GSH is bound, and 2) the helix $\alpha4'$, which closes the presumed electrophilic substrate binding site and involves a basic side chain in the anion binding site of the enzyme. Based on structural alignments, all five *P. chrysosporium* GSTs from this class should share the same original properties, allowing us to define a new structural GST class with a novel dimerization mode. This class holds the unique property of having conserved all the secondary structures of monomeric glutaredoxin 2, which is the presumed common ancestor of the cytosolic GSTs (43). All other structures solved so far lost at least helix $\alpha4'$. The catalytic Ser-22 is in hydrogen-bonding contact with the thiol sulfur atom of the cysteinyl moiety of GSH and thus could participate in the stabilization of the thiolate anion. The GST5118-S22A mutant retains the ability to conjugate GSH onto electrophilic substrates and exhibits weak peroxidase and thiol transferase activities. This suggests that another residue could stabilize the thiolate form of GSH and thus lower its pK_a. In the vicinity of GSH, Asn-24 which is conserved in isoforms of this class (supplemental Fig. S6) could fulfill this role with few conformational changes. In accordance, this Asn residue is conserved in Ure2p class and has been shown to be crucial for peroxidase activity of *Saccharomyces cerevisiae* Ure2p (55). This observation could explain why GST5118-S22A shows such an activity pattern.

A sulfate binding pocket was identified in the N-terminal domain of GST5118 structure, close to the GSH binding site. This could explain the binding of ANS, which possesses a sulfonic acid moiety, at the G site and the competition between ANS and GSH. The unique binding mode of ANS onto GST5118 allowed us to use it as a ligand screening tool. Glutathionylated and sulfur-containing compounds as well as products resulting from wood degradation compete with ANS, suggesting that all of them bind at the G site. This is in accordance

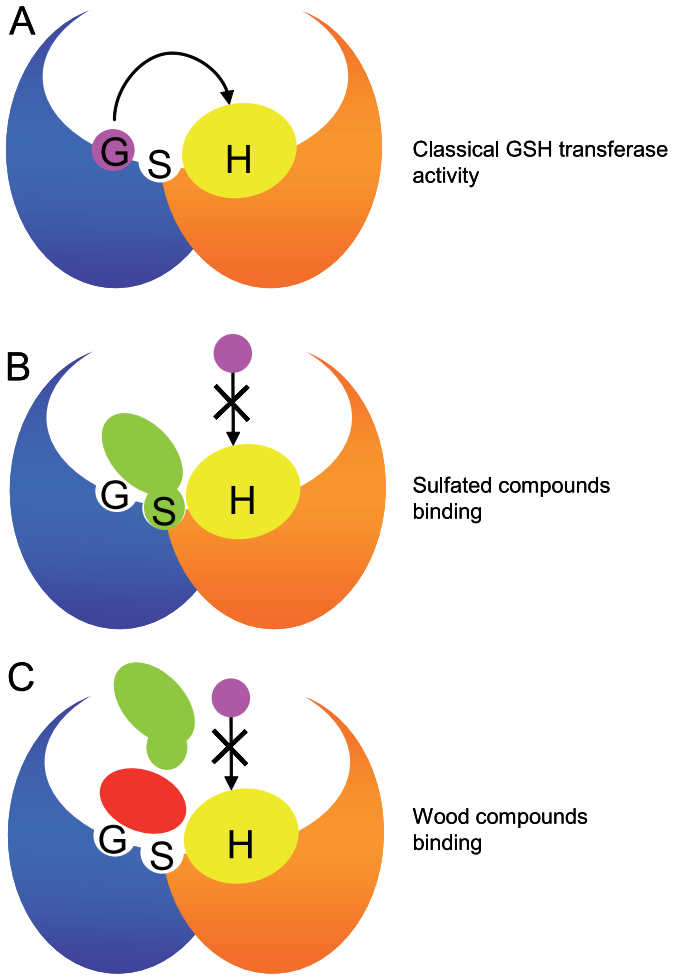

FIGURE 5. **Schematic representation of compounds binding onto GST5118 monomer.** The N-terminal domain containing the GSH binding site (*G*) as well as the ANS and sulfated compound binding site (*S*) is depicted in *blue* (on the *left*), whereas the C-terminal domain containing the substrate binding site (*H*) is depicted in *orange* (on the right). Binding of both GSH (*pink*) and substrate (*yellow*) in their respective sites (*A*) enables the classical GSH transferase activity of the enzyme. Binding of ANS and sulfated compounds in the S site (*B*) or binding of non-substrate wood compounds (*red*) in the N-terminal domain (*C*) inhibits the GSH binding but does not affect substrate binding and alters the GSH transferase activity of the enzyme.

with the structural data concerning glutathionylated and sulfated compounds; however, it was unexpected for wood compounds because the recognition of hydrophobic substrates has never been described to occur at the G site.

The consequence of binding wood compounds at the G site is the inability of GST5118 to accept and therefore transfer GSH anymore. This enzyme could thus have two functions, possibly depending on the intracellular concentration of GSH and wood compounds: a classical GSH transferase activity, especially with phenethyl-ITC as substrate, and a ligandin property toward wood extractive compounds. The affinity for ligand binding is likely to be driven by very fine interactions. An example of this fine ligand specificity is the pair vanillin/vanillic acid, in which the first compound is well recognized by GST5118, whereas the latter cannot displace ANS. The only difference between these two molecules is the addition of a single atom of oxygen, transforming the aldehyde function into an acidic one. Vanillin is

known to be one of the key intermediates found during wood decay, and it was shown to be taken up by fungal cells (56). However, vanillin is not a nutrient substrate but rather acts as a chemical stress on fungal cells (57). It has also been suggested that it can be responsible for activation of fungal metabolic pathways for phenolic compounds (58). This ligandin property of GST5118 could thus be helpful to protect the cell against highly reactive xenobiotics or secondary metabolites. Similar functions were assigned to plant Phi and Tau GSTs that participate in the transport of highly reactive products to the vacuole without catalyzing their conjugation and thus sequestering them away from critical intracellular targets (59, 60).

In conclusion, the structural and functional properties of GST5118 allow us to define a new GST class that we name GSTFuA (for fungal specific class A). Accordingly, GST5118 from *P. chrysosporium* can thus be renamed GSTFuA1.

Acknowledgments—We thank the staffs of the BM30A beamline at the European Synchrotron Radiation Facility (Grenoble, France) and the Proxima 1 beamline at SOLEIL (Gif-sur-Yvette, France) for kind assistance during data collection.

REFERENCES

1. Hayes, J. D., Flanagan, J. U., and Jowsey, I. R. (2005) Glutathione transferases. *Annu. Rev. Pharmacol. Toxicol.* **45,** 51–88
2. Mannervik, B. (2012) Five decades with glutathione and the GSTome. *J. Biol. Chem.* **287,** 6072–6083
3. Oakley, A. J., Lo Bello, M., Nuccetelli, M., Mazzetti, A. P., and Parker, M. W. (1999) The ligandin (non-substrate) binding site of human Pi class glutathione transferase is located in the electrophile binding site (H-site). *J. Mol. Biol.* **291,** 913–926
4. Lederer, B., and Böger, P. (2003) Binding and protection of porphyrins by glutathione *S*-transferases of *Zea mays* L. *Biochim. Biophys. Acta* **1621,** 226–233
5. Dixon, D. P., Lapthorn, A., Madesis, P., Mudd, E. A., Day, A., and Edwards, R. (2008) Binding and glutathione conjugation of porphyrinogens by plant glutathione transferases. *J. Biol. Chem.* **283,** 20268–20276
6. Bilang, J., Macdonald, H., King, P. J., and Sturm, A. (1993) A soluble auxin-binding protein from *Hyoscyamus muticus* is a glutathione *S*-transferase. *Plant Physiol.* **102,** 29–34
7. Conn, S., Curtin, C., Bézier, A., Franco, C., and Zhang, W. (2008) Purification, molecular cloning, and characterization of glutathione *S*-transferases (GSTs) from pigmented *Vitis vinifera* L. cell suspension cultures as putative anthocyanin transport proteins. *J. Exp. Bot.* **59,** 3621–3634
8. Morel, M., Ngadin, A. A., Droux, M., Jacquot, J. P., and Gelhaye, E. (2009) The fungal glutathione *S*-transferase system. Evidence of new classes in the wood-degrading basidiomycete *Phanerochaete chrysosporium*. *Cell Mol. Life Sci.* **66,** 3711–3725
9. Thuillier, A., Ngadin, A. A., Thion, C., Billard, P., Jacquot, J. P., Gelhaye, E., and Morel, M. (2011) Functional diversification of fungal glutathione transferases from the ure2p class. *Int. J. Evol. Biol.* **2011,** 938308
10. McGoldrick, S., O'Sullivan, S. M., and Sheehan, D. (2005) Glutathione transferase-like proteins encoded in genomes of yeasts and fungi. Insights into evolution of a multifunctional protein superfamily. *FEMS Microbiol. Lett.* **242,** 1–12
11. Lian, H. Y., Jiang, Y., Zhang, H., Jones, G. W., and Perrett, S. (2006) The yeast prion protein Ure2. Structure, function, and folding. *Biochim. Biophys. Acta* **1764,** 535–545
12. Garcerá, A., Barreto, L., Piedrafita, L., Tamarit, J., and Herrero, E. (2006) *Saccharomyces cerevisiae* cells have three Omega class glutathione *S*-transferases acting as 1-Cys thiol transferases. *Biochem. J.* **398,** 187–196
13. Choi, J. H., Lou, W., and Vancura, A. (1998) A novel membrane-bound glutathione *S*-transferase functions in the stationary phase of the yeast *Saccharomyces cerevisiae*. *J. Biol. Chem.* **273,** 29915–29922
14. Fraser, J. A., Davis, M. A., and Hynes, M. J. (2002) A gene from *Aspergillus nidulans* with similarity to URE2 of *Saccharomyces cerevisiae* encodes a glutathione *S*-transferase which contributes to heavy metal and xenobiotic resistance. *Appl. Environ. Microbiol.* **68,** 2802–2808
15. Burns, C., Geraghty, R., Neville, C., Murphy, A., Kavanagh, K., and Doyle, S. (2005) Identification, cloning, and functional expression of three glutathione transferase genes from *Aspergillus fumigatus*. *Fungal Genet. Biol.* **42,** 319–327
16. Meux, E., Prosper, P., Ngadin, A., Didierjean, C., Morel, M., Dumarçay, S., Lamant, T., Jacquot, J. P., Favier, F., and Gelhaye, E. (2011) Glutathione transferases of *Phanerochaete chrysosporium*. *S*-Glutathionyl-*p*-hydroquinone reductase belongs to a new structural class. *J. Biol. Chem.* **286,** 9162–9173
17. Masai, E., Ichimura, A., Sato, Y., Miyauchi, K., Katayama, Y., and Fukuda, M. (2003) Roles of the enantioselective glutathione *S*-transferases in cleavage of β-aryl ether. *J. Bacteriol.* **185,** 1768–1775
18. Lee, S., Monnappa, A. K., and Mitchell, R. J. (2012) Biological activities of lignin hydrolysate-related compounds. *BMB Rep.* **45,** 265–274
19. Lee, C. Y., Sharma, A., Cheong, J. E., and Nelson, J. L. (2009) Synthesis and antioxidant properties of dendritic polyphenols. *Bioorg. Med. Chem. Lett.* **19,** 6326–6330
20. Schenk, P. M., Baumann, S., Mattes, R., and Steinbiss, H. H. (1995) Improved high level expression system for eukaryotic genes in *Escherichia coli* using T7 RNA polymerase and rare ArgtRNAs. *BioTechniques* **19,** 196–198, 200
21. D'Ambrosio, K., Kauffmann, B., Rouhier, N., Benedetti, E., Jacquot, J. P., Aubry, A., and Corbier, C. (2003) Crystallization and preliminary x-ray studies of the glutaredoxin from poplar in complex with glutathione. *Acta Crystallogr. D Biol. Crystallogr* **59,** 1043–1045
22. Couturier, J., Koh, C. S., Zaffagnini, M., Winger, A. M., Gualberto, J. M., Corbier, C., Decottignies, P., Jacquot, J. P., Lemaire, S. D., Didierjean, C., and Rouhier, N. (2009) Structure-function relationship of the chloroplastic glutaredoxin S12 with an atypical WCSYS active site. *J. Biol. Chem.* **284,** 9299–9310
23. Zhang, J., Shibata, A., Ito, M., Shuto, S., Ito, Y., Mannervik, B., Abe, H., and Morgenstern, R. (2011) Synthesis and characterization of a series of highly fluorogenic substrates for glutathione transferases, a general strategy. *J. Am. Chem. Soc.* **133,** 14109–14119
24. Kim, D. E., Kim, K. H., Bae, Y. J., Lee, J. H., Jang, Y. H., and Nam, S. W. (2005) Purification and characterization of the recombinant arylsulfatase cloned from *Pseudoalteromonas carrageenovora*. *Protein Expr. Purif.* **39,** 107–115
25. Koh, C. S., Navrot, N., Didierjean, C., Rouhier, N., Hirasawa, M., Knaff, D. B., Wingsle, G., Samian, R., Jacquot, J. P., Corbier, C., and Gelhaye, E. (2008) An atypical catalytic mechanism involving three cysteines of thioredoxin. *J. Biol. Chem.* **283,** 23062–23072
26. Kabsch, W. (2010) XDS. *Acta Crystallogr. D Biol. Crystallogr.* **66,** 125–132
27. Evans, P. (2006) Scaling and assessment of data quality. *Acta Crystallogr. D Biol. Crystallogr.* **62,** 72–82
28. Winn, M. D., Ballard, C. C., Cowtan, K. D., Dodson, E. J., Emsley, P., Evans, P. R., Keegan, R. M., Krissinel, E. B., Leslie, A. G., McCoy, A., McNicholas, S. J., Murshudov, G. N., Pannu, N. S., Potterton, E. A., Powell, H. R., Read, R. J., Vagin, A., and Wilson, K. S. (2011) Overview of the CCP4 suite and current developments. *Acta Crystallogr. D Biol. Crystallogr.* **67,** 235–242
29. Adams, P. D., Afonine, P. V., Bunkóczi, G., Chen, V. B., Davis, I. W., Echols, N., Headd, J. J., Hung, L. W., Kapral, G. J., Grosse-Kunstleve, R. W., McCoy, A. J., Moriarty, N. W., Oeffner, R., Read, R. J., Richardson, D. C., Richardson, J. S., Terwilliger, T. C., and Zwart, P. H. (2010) PHENIX. A comprehensive Python-based system for macromolecular structure solution. *Acta Crystallogr. D Biol. Crystallogr.* **66,** 213–221
30. Terwilliger, T. (2004) SOLVE and RESOLVE. Automated structure solution, density modification, and model building. *J. Synchrotron Radiat.* **11,** 49–52
31. Emsley, P., Lohkamp, B., Scott, W. G., and Cowtan, K. (2010) Features and development of Coot. *Acta Crystallogr. D Biol. Crystallogr.* **66,** 486–501
32. Chen, V. B., Arendall, W. B., 3rd, Headd, J. J., Keedy, D. A., Immormino, R. M., Kapral, G. J., Murray, L. W., Richardson, J. S., and Richardson, D. C.

(2010) MolProbity. All-atom structure validation for macromolecular crystallography. *Acta Crystallogr. D Biol. Crystallogr.* **66,** 12–21
33. Krissinel, E., and Henrick, K. (2007) Inference of macromolecular assemblies from crystalline state. *J. Mol. Biol.* **372,** 774–797
34. Holm, L., and Rosenström, P. (2010) Dali server. Conservation mapping in 3D. *Nucleic Acids Res.* **38,** W545–W549
35. Gille, C. (2006) Structural interpretation of mutations and SNPs using STRAP-NT. *Protein Sci.* **15,** 208–210
36. Cole, C., Barber, J. D., and Barton, G. J. (2008) The Jpred 3 secondary structure prediction server. *Nucleic Acids Res.* **36,** W197–W201
37. Gouet, P., Robert, X., and Courcelle, E. (2003) ESPript/ENDscript. Extracting and rendering sequence and 3D information from atomic structures of proteins. *Nucleic Acids Res.* **31,** 3320–3323
38. Allocati, N., Casalone, E., Masulli, M., Ceccarelli, I., Carletti, E., Parker, M. W., and Di Ilio, C. (1999) Functional analysis of the evolutionarily conserved proline 53 residue in *Proteus mirabilis* glutathione transferase B1-1. *FEBS Lett.* **445,** 347–350
39. Cocco, R., Stenberg, G., Dragani, B., Rossi Principe, D., Paludi, D., Mannervik, B., and Aceto, A. (2001) The folding and stability of human Alpha class glutathione transferase A1-1 depend on distinct roles of a conserved N-capping box and hydrophobic staple motif. *J. Biol. Chem.* **276,** 32177–32183
40. Skopelitou, K., Dhavala, P., Papageorgiou, A. C., and Labrou, N. E. (2012) A glutathione transferase from *Agrobacterium tumefaciens* reveals a novel class of bacterial GST superfamily. *PLoS ONE* **7,** e34263
41. Reinemer, P., Prade, L., Hof, P., Neuefeind, T., Huber, R., Zettl, R., Palme, K., Schell, J., Koelln, I., Bartunik, H. D., and Bieseler, B. (1996) Three-dimensional structure of glutathione *S*-transferase from *Arabidopsis thaliana* at 2.2 Å resolution. Structural characterization of herbicide-conjugating plant glutathione *S*-transferases and a novel active site architecture. *J. Mol. Biol.* **255,** 289–309
42. Xia, B., Vlamis-Gardikas, A., Holmgren, A., Wright, P. E., and Dyson, H. J. (2001) Solution structure of Escherichia coli glutaredoxin-2 shows similarity to mammalian glutathione *S*-transferases. *J. Mol. Biol.* **310,** 907–918
43. Frova, C. (2006) Glutathione transferases in the genomics era. New insights and perspectives. *Biomol. Eng.* **23,** 149–169
44. Sinning, I., Kleywegt, G. J., Cowan, S. W., Reinemer, P., Dirr, H. W., Huber, R., Gilliland, G. L., Armstrong, R. N., Ji, X., and Board, P. G. (1993) Structure determination and refinement of human Alpha class glutathione transferase A1-1 and a comparison with the Mu and Pi class enzymes. *J. Mol. Biol.* **232,** 192–212
45. Rossjohn, J., McKinstry, W. J., Oakley, A. J., Verger, D., Flanagan, J., Chelvanayagam, G., Tan, K. L., Board, P. G., and Parker, M. W. (1998) Human Theta class glutathione transferase. The crystal structure reveals a sulfate-binding pocket within a buried active site. *Structure* **6,** 309–322
46. Board, P. G., Coggan, M., Chelvanayagam, G., Easteal, S., Jermiin, L. S., Schulte, G. K., Danley, D. E., Hoth, L. R., Griffor, M. C., Kamath, A. V., Rosner, M. H., Chrunyk, B. A., Perregaux, D. E., Gabel, C. A., Geoghegan, K. F., and Pandit, J. (2000) Identification, characterization, and crystal structure of the Omega class glutathione transferases. *J. Biol. Chem.* **275,** 24798–24806
47. Agianian, B., Tucker, P. A., Schouten, A., Leonard, K., Bullard, B., and Gros, P. (2003) Structure of a *Drosophila* Sigma class glutathione *S*-transferase reveals a novel active site topography suited for lipid peroxidation products. *J. Mol. Biol.* **326,** 151–165
48. Dirr, H., Reinemer, P., and Huber, R. (1994) X-ray crystal structures of cytosolic glutathione *S*-transferases. Implications for protein architecture, substrate recognition, and catalytic function. *Eur. J. Biochem.* **220,** 645–661
49. Menchise, V., Corbier, C., Didierjean, C., Jacquot, J. P., Benedetti, E., Saviano, M., and Aubry, A. (2000) Crystal structure of the W35A mutant thioredoxin h from *Chlamydomonas reinhardtii*. The substitution of the conserved active site Trp leads to modifications in the environment of the two catalytic cysteines. *Biopolymers* **56,** 1–7
50. Lillig, C. H., Berndt, C., and Holmgren, A. (2008) Glutaredoxin systems. *Biochim. Biophys. Acta* **1780,** 1304–1317
51. Polekhina, G., Board, P. G., Blackburn, A. C., and Parker, M. W. (2001) Crystal structure of maleylacetoacetate isomerase/glutathione transferase Zeta reveals the molecular basis for its remarkable catalytic promiscuity. *Biochemistry* **40,** 1567–1576
52. Jeppesen, M. G., Ortiz, P., Shepard, W., Kinzy, T. G., Nyborg, J., and Andersen, G. R. (2003) The crystal structure of the glutathione *S*-transferase-like domain of elongation factor 1Bγ from *Saccharomyces cerevisiae*. *J. Biol. Chem.* **278,** 47190–47198
53. Masai, E., Katayama, Y., Kubota, S., Kawai, S., Yamasaki, M., and Morohoshi, N. (1993) A bacterial enzyme degrading the model lignin compound β-etherase is a member of the glutathione *S*-transferase superfamily. *FEBS Lett.* **323,** 135–140
54. Schonbrunn, E., Eschenburg, S., Luger, K., Kabsch, W., and Amrhein, N. (2000) Structural basis for the interaction of the fluorescence probe 8-anilino-1-naphthalene sulfonate (ANS) with the antibiotic target MurA. *Proc. Natl. Acad. Sci. U.S.A.* **97,** 6345–6349
55. Zhang, Z. R., Bai, M., Wang, X. Y., Zhou, J. M., and Perrett, S. (2008) "Restoration" of glutathione transferase activity by single-site mutation of the yeast prion protein Ure2. *J. Mol. Biol.* **384,** 641–651
56. Shimizu, M., Kobayashi, Y., Tanaka, H., and Wariishi, H. (2005) Transportation mechanism for vanillin uptake through fungal plasma membrane. *Appl. Microbiol. Biotechnol.* **68,** 673–679
57. Shimizu, M., Yuda, N., Nakamura, T., Tanaka, H., and Wariishi, H. (2005) Metabolic regulation at the tricarboxylic acid and glyoxylate cycles of the lignin-degrading basidiomycete *Phanerochaete chrysosporium* against exogenous addition of vanillin. *Proteomics* **5,** 3919–3931
58. Nakamura, T., Ichinose, H., and Wariishi, H. (2012) Flavin-containing monooxygenases from *Phanerochaete chrysosporium* responsible for fungal metabolism of phenolic compounds. *Biodegradation* **23,** 343–350
59. Marrs, K. A., Alfenito, M. R., Lloyd, A. M., and Walbot, V. (1995) A glutathione *S*-transferase involved in vacuolar transfer encoded by the maize gene *Bronze-2*. *Nature* **375,** 397–400
60. Kitamura, S., Shikazono, N., and Tanaka, A. (2004) TRANSPARENT TESTA 19 is involved in the accumulation of both anthocyanins and proanthocyanidins in *Arabidopsis*. *Plant J.* **37,** 104–114

Characterization of a *Phanerochaete chrysosporium* Glutathione Transferase Reveals a Novel Structural and Functional Class with Ligandin Properties

Yann Mathieu, Pascalita Prosper, Marc Buée, Stéphane Dumarçay, Frédérique Favier, Eric Gelhaye, Philippe Gérardin, Luc Harvengt, Jean-Pierre Jacquot, Tiphaine Lamant, Edgar Meux, Sandrine Mathiot, Claude Didierjean and Mélanie Morel

J. Biol. Chem. 2012, 287:39001-39011.
doi: 10.1074/jbc.M112.402776 originally published online September 24, 2012
